Analysis of sample three-dimensional metrology data

~robert/sim/3d-met/draft10/analysis10.tex

Andy Kuhnert Robert Spero

30 October, 1997

Abstract

We analyze data from recent experiments conducted by Yekta Gürsel in which a corner cube was moved approximately 23 microns and the readouts from four gauges on a reference plate were recorded. The measurements were done in still air in July, 1997. We solve for the best fit of the three coordinates of motion of the corner cube, using data from all four gauges. The overall accuracy of the measurement is approximately ± 25 nm, attributable to surveying errors of approximately ± 3 mm. The noise inherent in the gauges corresponds to approximately 500 pm rms accuracy of the estimate of motion.

Part I
Setup and Data

1 Experimental Setup

The objective of the 3-D metrology experiment is to determine the motion of a test point to high precision by measuring the change in path lengths of laser beams connecting it to several reference points. The test point and reference point positions are defined by corner-cube reflectors.

The data analyzed here were collected in still air in July, 1997, over a duration of approximately 500 seconds. The experiment was built and run by Yekta Gürsel; the calculations in Part II are after [HCWP92], and the calculations in Part III are after [Gür97].

As shown in Figure 1, there are N static reference points, roughly in a plane. Three reference points are adequate to perform the measurement; the apparatus has five to allow for consistency checks, but only four data sets are currently available. One of the laser beams between the test point starting position and a reference point is shown as a vector $\vec{\mathbf{L}}_\mathbf{i}$; N such vectors make up the survey matrix. As the test point moves by $\vec{\delta}$, the length of each beam path l_i is read by a separate "heterodyne metrology gauge." Figure 2 shows the coordinate system and labeling of corner cubes.

The analysis presented here answers two questions: What is the inherent accuracy of the gauge data? What is the minimum correction to the survey necessary for consistency with the gauge data?

In Part II we describe the geometry in terms of vectors and use conventional data-fitting and error-estimation algorithms. In Part III the geometry is described in terms of tetrahedra formed

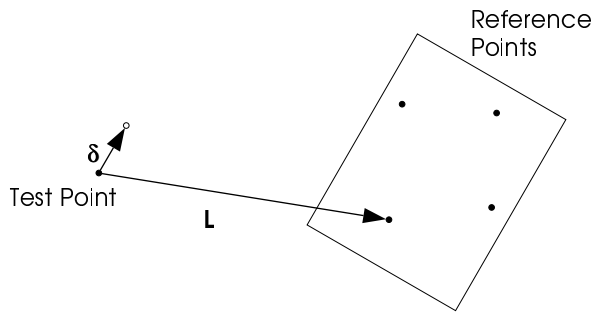

Figure 1: Measurement geometry. A survey vector $\vec{\mathbf{L_i}}$ from the initial position of the test point to one of the reference points is shown. The vector displacement (final - initial) of the test point is $\vec{\delta}$; for the data analyzed here, $|\mathbf{L}| \approx 80\,\mathrm{cm}$, $|\vec{\delta}| \approx 20$ microns. The angle between $\vec{\delta}$ and $\vec{\mathbf{L_i}}$ is shown exaggerated; the actual direction of motion of the test point is toward the center of the reference plate, within a few degrees.

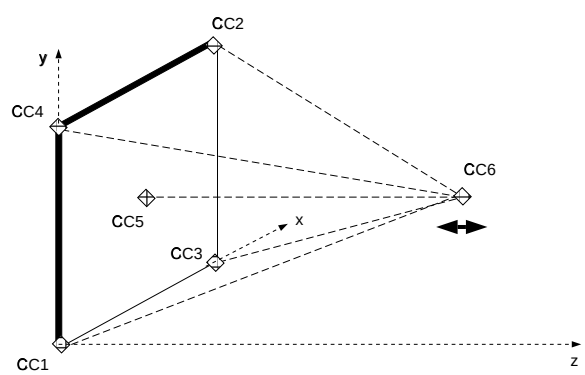

Figure 2: Coordinates and labeling of corner cubes.

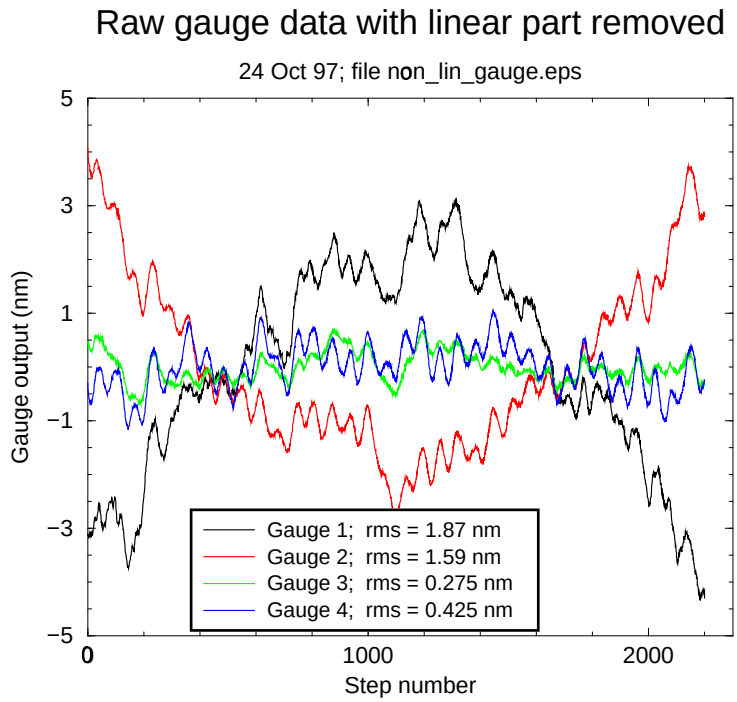

Figure 3: Data from four gauge heads after cyclic averaging and subtraction of linear part.

by combinations of gauges and a customized iterative numerical technique is used for the error analysis. The two methods give consistent results.

2 Cyclic-averaged data

The gauge outputs are recorded as the test point moves in steps. These data are pre-processed by "cyclic averaging."[1] Figure 3 shows the raw gauge data after subtraction of the straight line part. The data segment[2], of approximately 500 seconds duration, was selected to be relatively free of the effects of slamming doors and similar disturbances. The observed fluctuations are attributable to a combination of noise in the gauges and actual "noise" in the test point displacement.

There is an expected geometric effect giving a departure from linearity of magnitude

$$Q = \frac{|\vec{\delta}|^2 \sin^2 \psi}{2|\vec{\mathbf{L}}_\mathbf{i}|} \tag{1}$$

where ψ is the angle between the line of motion of the test point and $\vec{\mathbf{L}}_\mathbf{i}$. This gives $Q = 40\,\mathrm{pm}$ for the gauge with the largest ψ (approximately $15\,\mathrm{deg}$), small compared to the observed deviations from linear motion.

[1] Using Matlab code written by Stuart Shaklan.

[2] Data file /home/shaklan/microarc/3d/3dmgauge868378642.dat.

Part II
Vector Method

In this Part, we use the data from the gauge heads and information from the static survey to directly compute the motion of the test point. The geometry is described by vectors, with coordinates used only in the final stages of the numerical computation.

3 Analysis formulae

The response of the measurement gauges to motion of the test point is

$$l_i = |\vec{\mathbf{L}}_i + \vec{\delta}| - |\vec{\mathbf{L}}_i|. \tag{2}$$

Here the $|\ldots|$ symbol represents the vector norm operation. We initially assume that the $\vec{\mathbf{L}}_i$ are known from surveying and that the l_i are read from the metrology gauges without error. The common origin for all vectors is the starting position of the test point. When coordinates are introduced a right-handed coordinate system is used with the reference plate in the negative z direction relative to the origin, and with motion towards the plate giving positive δ_z.

3.1 Solving for test point motion

Equation 2 is non-linear, but as indicated in Section 2, the linear approximation is adequate for the data in hand.[3] Keeping only the linear (gauge slope) terms, Equation 2 simplifies to:

$$l_i = \hat{\mathbf{L}}_\mathbf{i} \cdot \vec{\delta} \tag{3}$$

where $\hat{\mathbf{L}}_\mathbf{i}$ is the unit vector from the test point to reference point i ($\hat{\mathbf{L}}_\mathbf{i} = \vec{\mathbf{L}}_\mathbf{i}/|\vec{\mathbf{L}}_\mathbf{i}|$) and the $\cdot$ symbol indicates the vector dot product. (Note that the scale of the surveying drops out; only the angles influence the gauges.)

Define the survey matrix:

$$\mathbf{L} = \frac{L_{ij}}{|\vec{\mathbf{L}}_\mathbf{i}|} \tag{4}$$

Here the i subscript identifies which reference point is measured, and the j subscript identifies which (x,y,z) coordinate.

Then

$$\vec{\mathbf{l}} = \mathbf{L} \cdot \vec{\delta} \tag{5}$$

where $\vec{\mathbf{l}}$ is the vector formed from the N fitted gauge slopes, and the $\cdot$ symbol represents a matrix-vector product.

Designate the solution of Equation 5 that uses all N gauges as $\vec{\delta}_4$. The equation is over-determined, and represents a data-fitting problem that can be solved by the Matlab least-squares matrix solve operator, "\".

[3] If the rms errors are reduced to a level comparable in magnitude to Q of Equation 1, the linear fit that determines the slope of the gauge outputs with test point motion can be modified to account for the known quadratic departure. This modification will improve the precision of the numerical method to the sub-picometer level.

3.2 Estimation of error in $\vec{\delta}$ and L

The accuracy of the solution is estimated in two ways: by evaluating the error

$$E = |\vec{\mathbf{l}} - \mathbf{L}\cdot\vec{\delta}_4|, \tag{6}$$

and by comparing solutions of Equation 5 found by using the full data set ($\vec{\delta}_4$) and various partial data sets formed by taking the elements of $\vec{\mathbf{l}}$ three at a time, each corresponding to the tetrahedron composed of three reference points and the test point ($\vec{\delta}_3$). The resulting error estimate is $\vec{\varepsilon} = \vec{\delta}_4 - \vec{\delta}_3$. E and $|\vec{\varepsilon}|$ should provide similar estimates of the accuracy of the fit solution $\vec{\delta}_4$.

We expect to find that E is dominated by inaccuracies in the survey matrix $\mathbf{L}$: surveying angular errors of magnitude θ cause errors of magnitude $E \approx \theta|\vec{\delta}|$. The uncertainty in the corner cube positions is on the order of 3 mm; on the 80 cm baseline this corresponds to $\theta \approx 3 \cdot 10^{-3}$ rad, or $E \approx 60$ nm.

As a check that non-zero E comes primarily from surveying errors, we fix $\vec{\delta}_4$ and $\vec{\mathbf{l}}$ and perturb the survey matrix $\mathbf{L}$ to minimize E defined by Equation 6. This minimization is readily accomplished by the Matlab function **fmins**. Designate the perturbed matrix $\mathbf{L}_{E=0}$; we expect to find that $\delta\mathbf{L} = \mathbf{L} - \mathbf{L}_{E=0}$ has elements on the order of 1 mm. There are twelve elements (eight of them independent—the two surveying angles per reference point) in $\mathbf{L}$ that are varied to minimize the scalar quantity E; therefore the adjusted solution is almost certainly not unique, and is therefore unphysical.

3.3 Simulation of the effect of gauge errors

From Figure 3, the rms noise in the gauge data is approximately 1 nm. This noise is the sum of noisy motion of the test point, and noise added by imperfections in the measurement. To derive an upper limit to the measurement noise, we assume that the test point motion is perfectly smooth and noise-free, and that all observed noise is due to errors in the measurement. We simulate this measurement noise by solving for $\vec{\delta}_4$ many times, taking the gauge data perturbed by a random amount each time. The perturbations are of magnitude 0.5 nm * RANDN, where RANDN is the Matlab function that produces randomly distributed random numbers with mean 0 and variance 1.0—this is equivalent to adding 1 nm rms noise to the gauges. The resulting upper limits to rms noise in the determination of $\vec{\delta}$ are 1.0, 0.95, and 0.27 nm for the x, y, and z components, respectively.

3.4 Simulation of the effect survey errors

Figure 4 illustrates the effect on E of perturbing all the coordinates of the test points in random directions by varying amounts, and Figure 5 histograms the results of a similar run. This randomized hunt found solutions starting at coordinate displacements around 0.7 mm. The range for the most probable solutions is 1–3 mm. The solutions at arbitrarily large displacements correspond to perturbing the positions of the corner cubes in a manner that preserves the surveying angles.

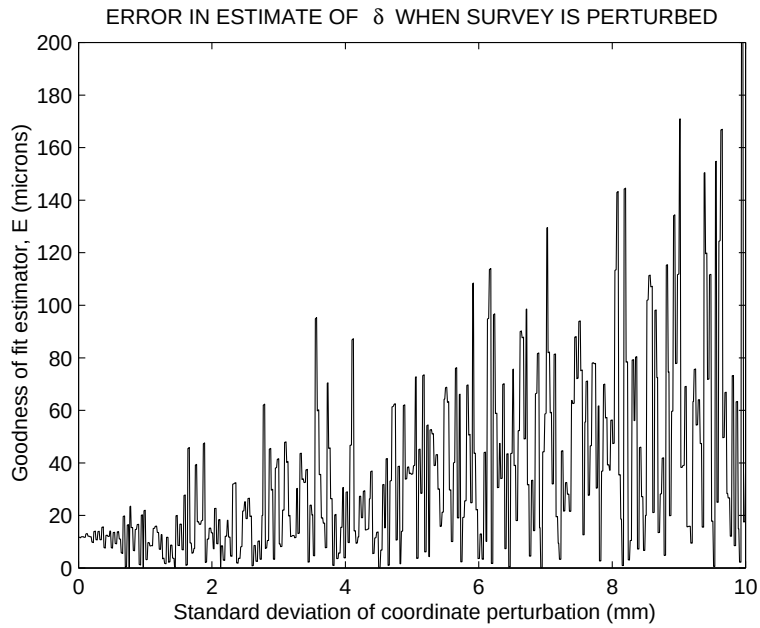

Figure 4: Illustration of how random deviations from the default surveying data affect E, (Equation 6), the accuracy of the estimate of $|\vec{\delta}|$. Each of the elements of $\mathbf{L}$ was perturbed a random amount with standard deviation varying from 0 to 10 mm in 0.1 mm steps.

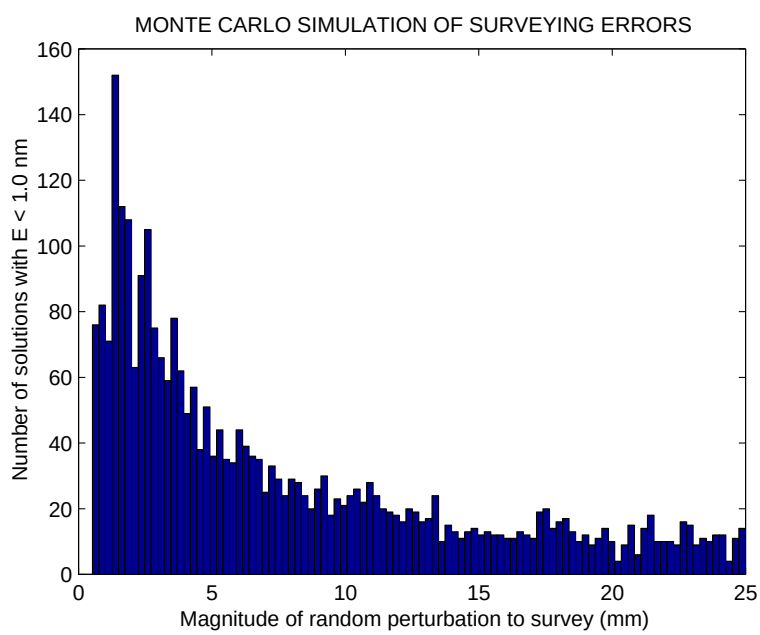

Figure 5: Histogram based on Monte Carlo simulation with perturbation steps of 0.1 nm. Values below the "solution threshold" of 1 nm are counted. The gap between 0.0 and 0.7 mm corresponds to the absence of solutions for this region in Figure 4.

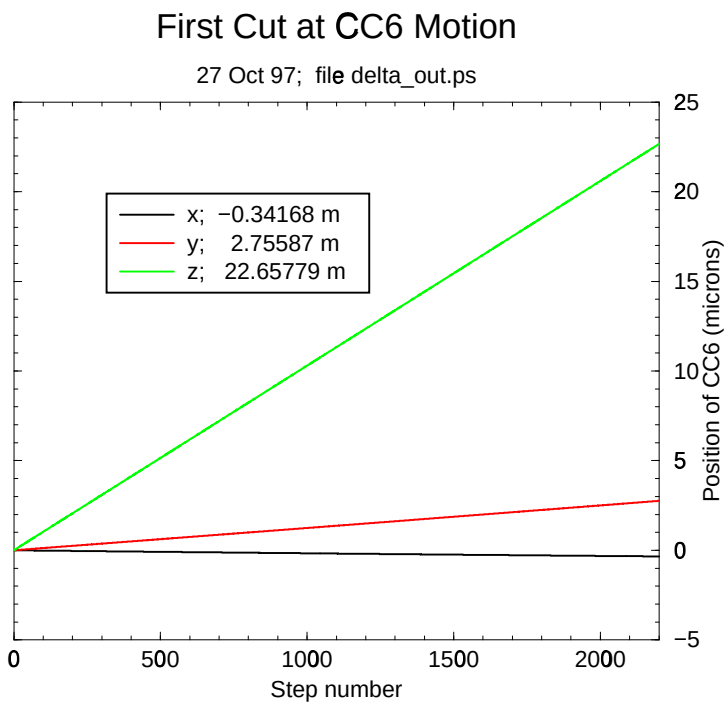

Figure 6: CC6 motion computed using all four gauge heads.

4 Numerical results

4.1 Calculation with measured survey

Figure 6 shows the computed motion, and Figure 7 shows the nonlinear part of that motion, both using all four gauges and the measured[4] survey matrix **L** Note that the z-motion follows a line more closely than x or y; this is due to feedback to Corner Cube 6 position, based on Gauge 5, that ensured linearity as the corner cube was stepped through its range. The deviations from linearity in the x and y directions evident in Figure 7 may be due to the geometry of the flexure mount used for the corner cube.

The residuals E are shown in Figure 8. As expected because of inaccuracies in the survey, the E are predominately linear in step number.

4.2 Calculation with artificial survey

Figure 9 shows the residuals in the gauge data after the survey numbers are adjusted to minimize E; the adjustments are on the order of 1–3 mm. The rms fluctuation in E is approximately 250 pm in each gauge. Figure 10 shows the difference $\vec{\varepsilon}$ between $\vec{\delta}_4$ and the $\vec{\delta}_3$ calculated from TH1; the magnitude of the largest component is approximately 500 pm, consistent with the gauge noise of Figure 9.

[4]These results are unchanged by the survey adjustment described below.

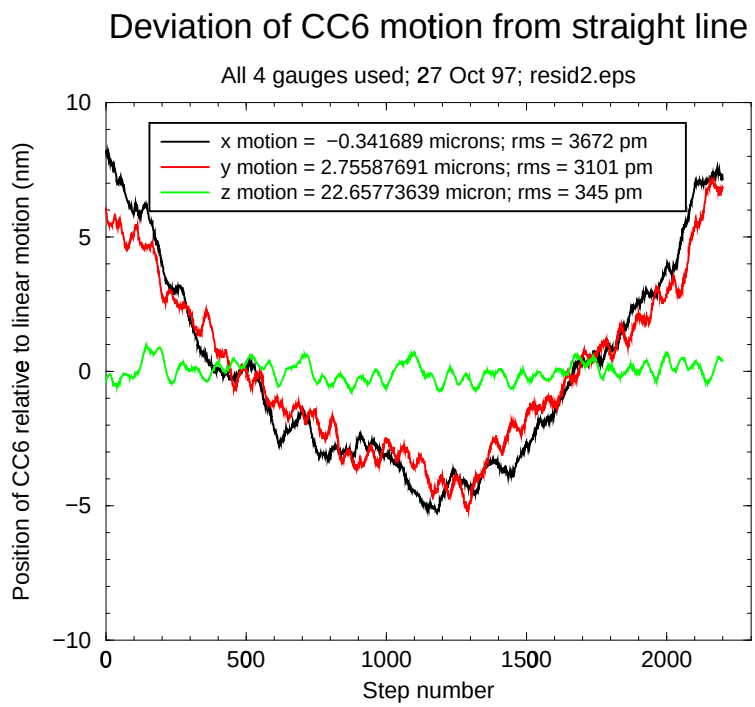

Figure 7: Data of Figure 6 with straight-line part removed and vertical scale magnified.

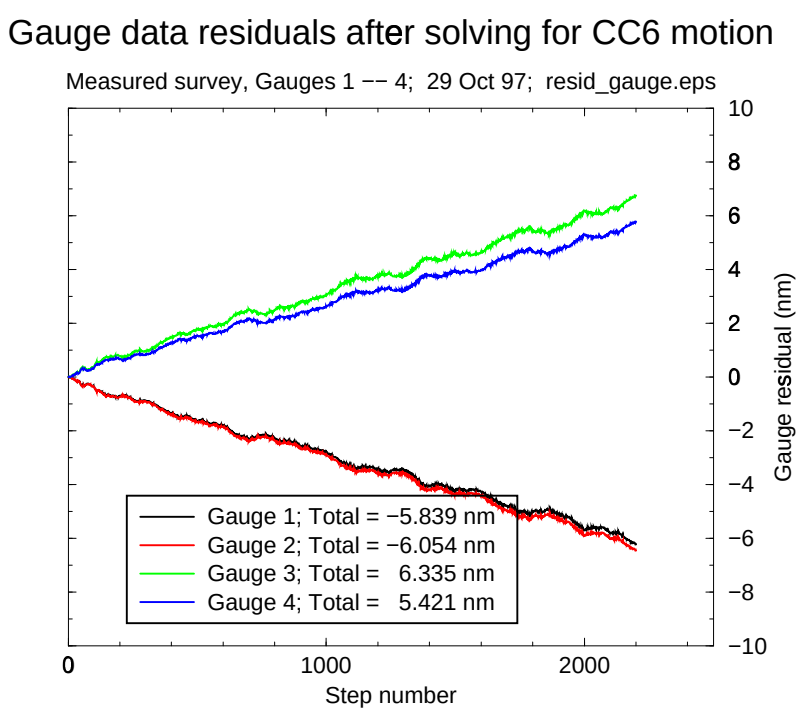

Figure 8: Residuals in gauge data, E, using original survey.

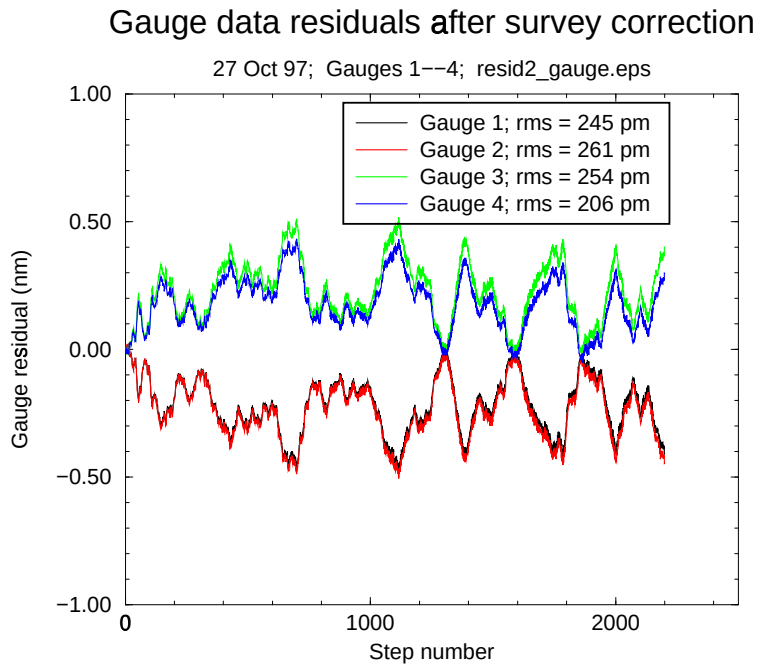

Figure 9: Residuals in gauge data, E, after survey adjustment.

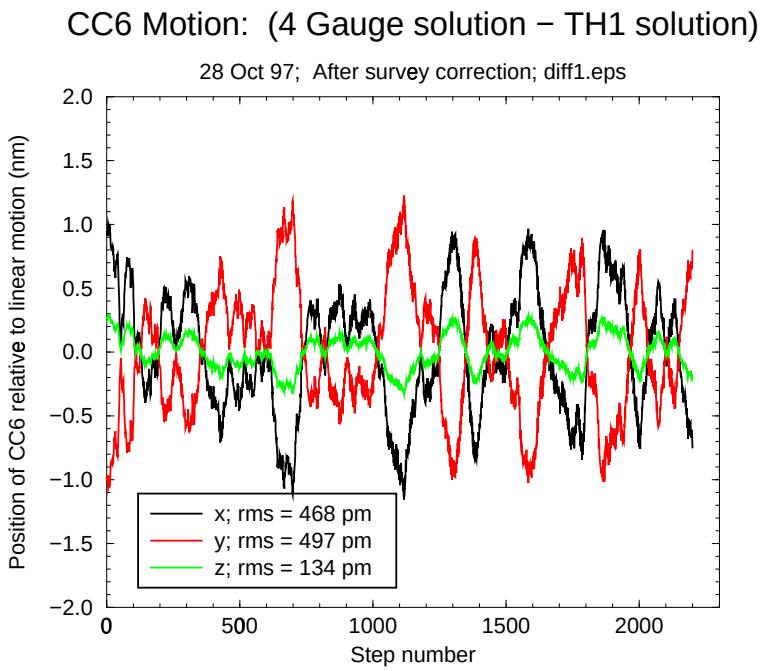

Figure 10: Difference between two solutions for motion of CC6: solution using all 4 gauges, and solution using the three gauges (1,2,3) composing TH1 (Figure 1), with survey correction applied.

4.3 Summary of test point motion calculations

1. In addition to the approximately 23 micron displacement perpendicular to the reference plane, there was approximately 3 micron displacement in the plane (Figure 6).

2. For the total 23 micron motion the E of four gauges ranges over ± 6 nm (Figure 8), and the variation $\vec{\varepsilon}$ ranges by ± 7 nm in the z-direction, ± 25 nm in the x- and y-directions. These errors are almost certainly due to errors in the survey.

3. The average of all four single-tetrahedron measurements $\vec{\delta}_3$ agrees (to better than 10 pm) with the four-gauge determination $\vec{\delta}_4$.

4. None of the $\vec{\delta}_3$ solutions stands out as being significantly different from the others; in this sense, none of the gauges can be singled out as anomalous.

5. The linear part of the variations $\vec{\varepsilon}$ and residuals E can eliminated by adjustments to the survey. The required adjustments for the 12 degrees of freedom of $\mathbf{L}$ range between 0.2 and 3 mm.

6. The least-squares determination of $\vec{\delta}_4$ is the same whether or not the $\Delta\mathbf{L}$ correction is applied. As expected, the mathematical survey correction does not improve the accuracy of the determination of the test point motion; this can be accomplished only by more accurate surveying.

TH (Outer)	Corner Cubes	TH (Inner)	Corner Cubes
1	1–2–3–6	5	1–3–5–6
2	1–2–4–6	6	2–3–5–6
3	1–3–4–6	7	2–4–5–6
4	2–3–4–6	8	1–4–5–6

Table 1: Corner cube assignments to the different tetrahedra (TH) used in the analysis of Part III.

Part III
Triangulation/Tetrahedron Method

In this Part we perform an alternative but equivalent analysis, in which the gauge data are grouped in triplets to form tetrahedra with the test point, Corner Cube 6 (CC6). Table 1 shows the tetrahedron designations (see Figure 2). The coordinate system and notation is the same as in Parts I and II, except the origin of coordinates is taken as CC1, so that motion of CC6 towards the plate results in negative δ_z.

The analysis focuses on the apparent differences in the position of CC6 computed using different tetrahedra. For each step in the motion of CC6, the geometry measured by the initial survey and the tetrahedron edge lengths measured by the gauges determine the three coordinates of CC6 by a triangulation computation. The motion of CC6 is very close to linear in step number, and therefore the slope of this motion for tetrahedron i, m_i, can be computed with high precision. If there are no errors in the survey or in the gauge outputs, the slope differences $S = m_i - m_j$ would all vanish. We see significant slope differences (Table 2). This can be explained by errors in the initial positions used for the triangulation. This analysis of the experimental data tried to establish if there is indeed a set of initial CC positions that:

1. Are consistent with the survey uncertainty of about ± 1 mm (A. Carlson, S.Shaklan).
2. Eliminate the slopes between the different solutions when determining CC6 x,y,z coordinates.

At first the initial survey of the CC's is used to triangulate CC6 position along its path of motion using the heterodyne gauge data (see Figure 11). This results in knowledge of its x,y,z motion to some accuracy. At the same time one can determine the slope differences S. All of that is now used to:

1. Calculate $\frac{\partial S}{\partial \mathrm{CC}}$ for any position shift ΔCC of each CC in x,y,z using the knowledge of CC6 x,y,z motion components.
2. Calculate changes to CC positions necessary to minimize slopes, by solving the matrix equation
$$\frac{\partial S}{\partial \mathrm{CC}} \cdot \Delta\mathrm{CC} = S$$
for ΔCC.

TH Pair	Slope Difference S (nm/micron) x	y	z
1-2	-2.018393	2.117414	-0.069839
1-3	-0.023386	2.127033	-0.609754
1-4	-2.194484	0.106363	-0.586079
2-3	1.995007	0.009619	-0.539915
2-4	-0.176091	-2.011051	-0.516240
3-4	-2.171098	-2.020670	0.023675
5-6	-0.425481	-0.398034	0.005221
5-7	-2.027428	1.542750	0.010261
5-8	-1.858390	1.699283	0.008191
6-7	-1.601947	1.940784	0.005041
6-8	-1.432908	2.097317	0.002971
7-8	0.169038	0.156533	-0.002070

Table 2: Slopes differences of CC6 motion (in units of nanometer/micron).

After applying these changes the program starts again using the new CC positions to get a more accurate estimate of the CC6 x,y,z motion repeating steps 1 and 2. Table 3 shows the results after five iterations.

Figures 12 and 13 show the difference in CC6 position between TH3 and TH4 in x,y and z initially and after five iterations. It is apparent that initially the difference increases linearly (slope) with the CC6 motion. In this particular example the program tried to minimize the slope differences S between TH6 and TH8 (inner TH). The offset of the data in Figure 13 is introduced by a linear fit to a slightly quadratic function and has no impact on this analysis.

References

[Gür97] Y. Gürsel. Metrology for spatial interferometry IV. *Proceedings of SPIE conference on Small Spacecraft, Space Environments and Instrumentation Technologies*, 3116, in press 1997.

[HCWP92] Brad Hines, Mark Colavita, Kent Wallace, and Andy Poulsen. Sub-nanometer laser metrology—some techniques and models. *Proceeding on high resolution imaging by interferometry, II Garching*, 1991

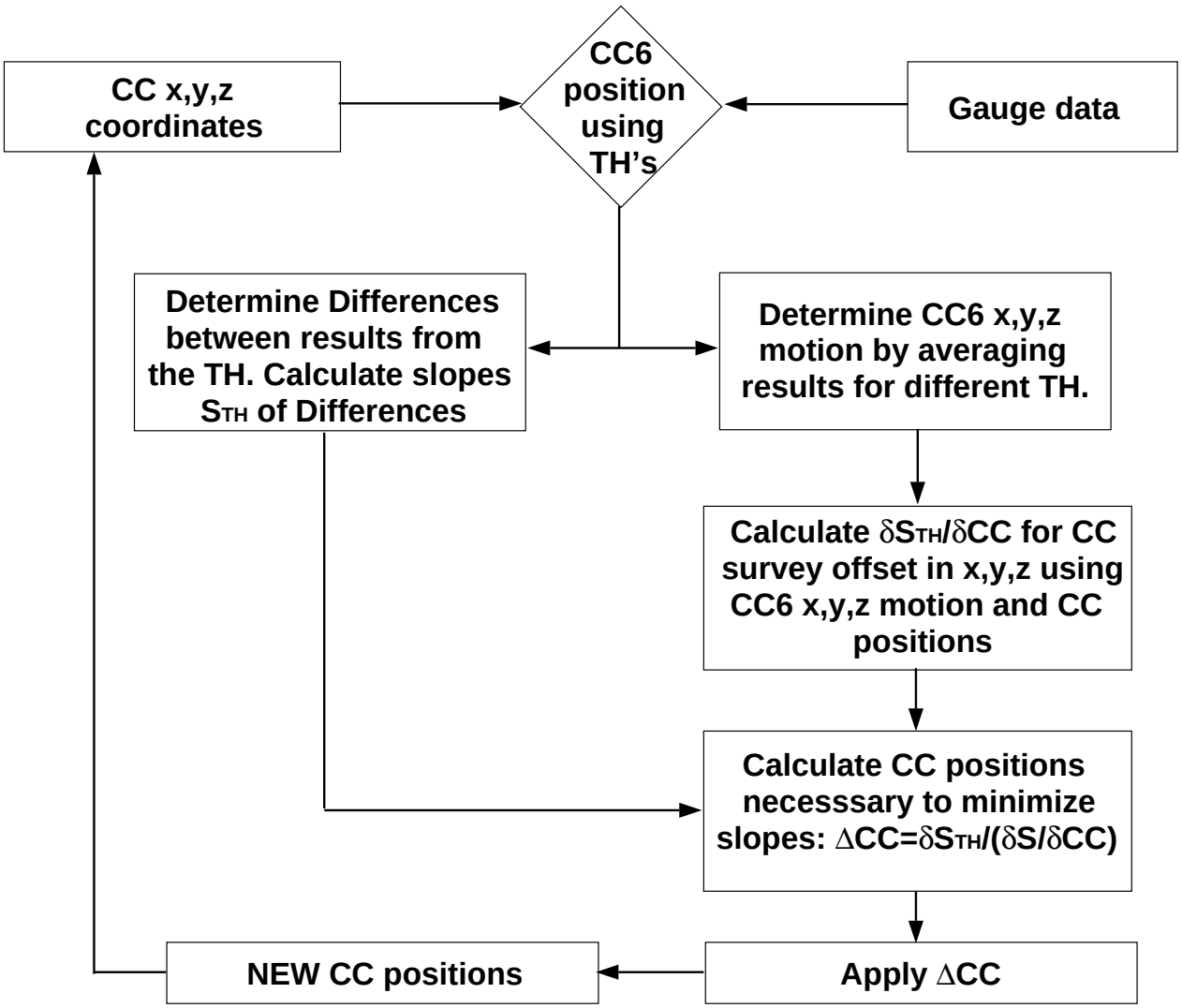

CC - corner cube
TH - tetrahedron, any 3 base plate corner cubes used to determine CC6 x.y.z coordinates.

Figure 11: Flow diagram for numerical solution by the triangulation/tetrahedron method.

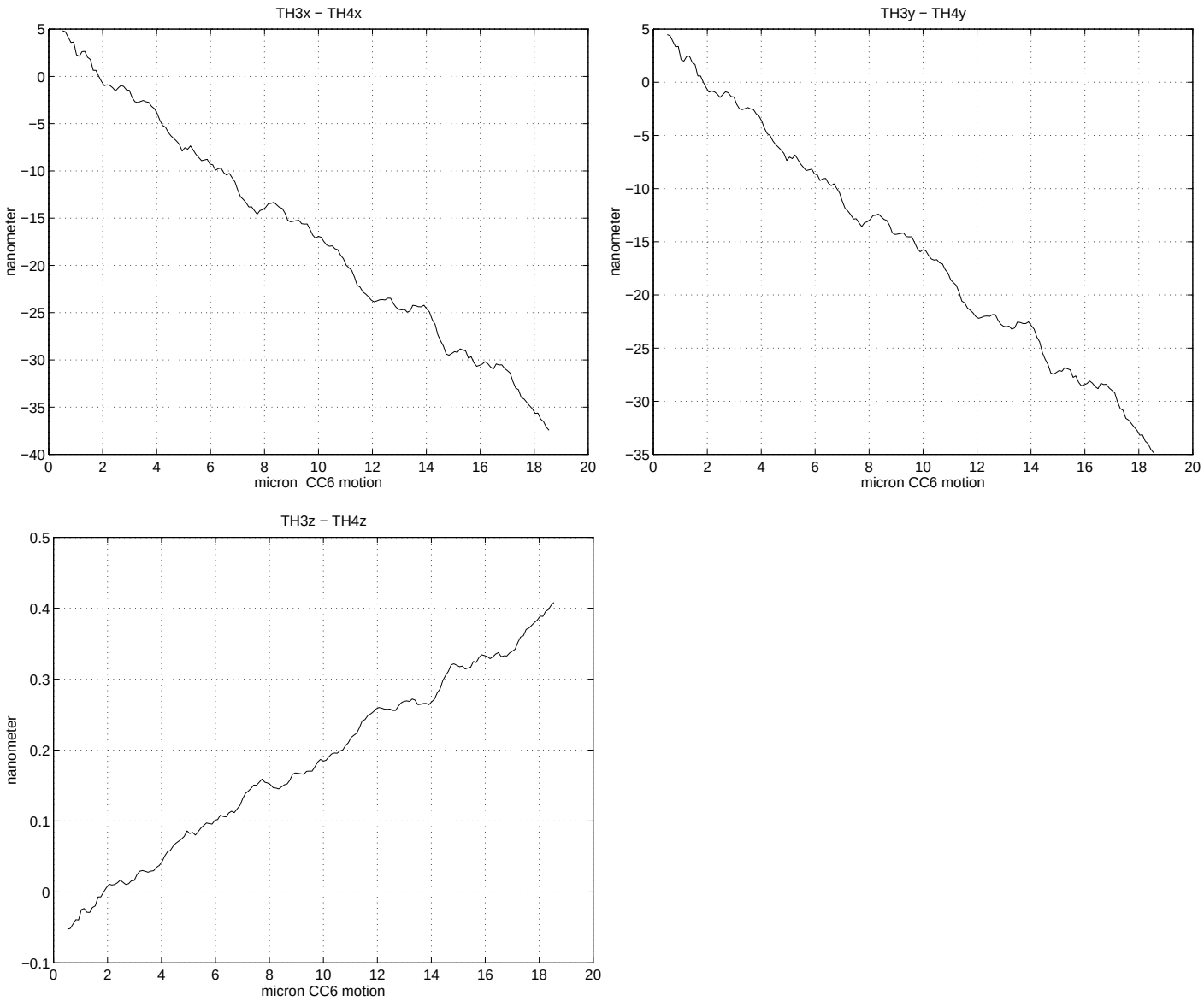

Figure 12: x,y,z components of *S* for TH 3 and 4 *before* modifying the surveyed CC positions.

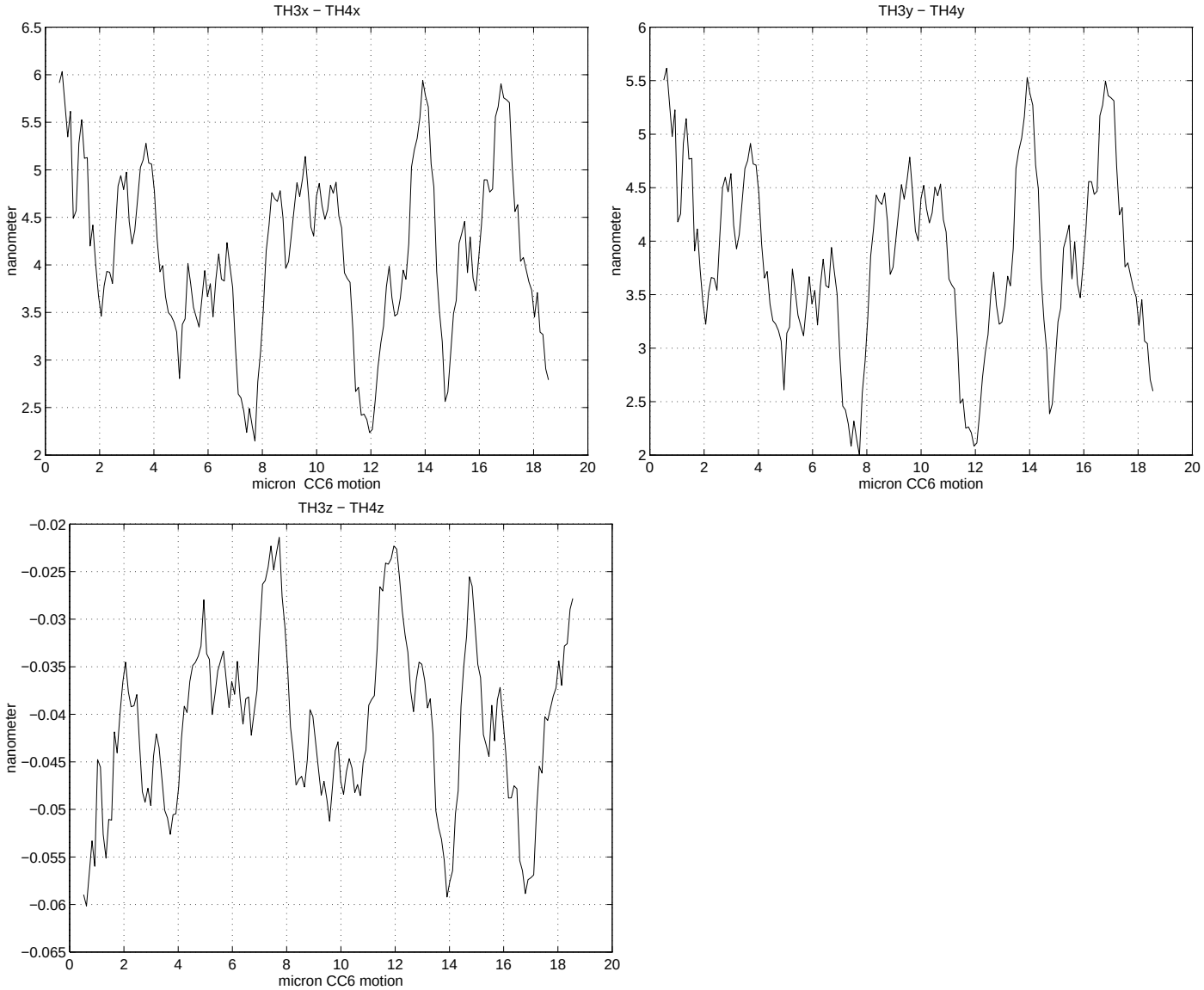

Figure 13: x,y,z components of *S* for TH 3 and 4 *after* modifying the surveyed CC positions.

TH	$\vec{\delta}$ (micron) x	y	z
1	0.341592708	-2.753849168	-22.662238719
2	0.341593889	-2.753850406	-22.662238665
3	0.341592721	-2.753850413	-22.662238382
4	0.341593995	-2.753849226	-22.662238403
5	0.341592574	-2.753835784	-22.662242720
6	0.341579003	-2.753848556	-22.662242638
7	0.341592575	-2.753865006	-22.662242815
8	0.341608485	-2.753850317	-22.662242913

TH Pair	Slope difference *S* (nm/micron) x	y	z
1–2	-0.000009	0.000009	-0.000001
1–3	-0.000000	0.000009	-0.000002
1–4	-0.000010	0.000000	-0.000001
2–3	0.000009	0.000000	-0.000001
2–4	-0.000001	-0.000009	-0.000000
3–4	-0.000009	-0.000009	0.000001
5–6	-0.000598	-0.000561	0.000011
5–7	-0.000060	-0.001211	0.000015
5–8	0.000629	-0.000575	0.000003
6–7	0.000538	-0.000650	0.000004
6–8	0.001226	-0.000014	-0.000008
7–8	0.000689	0.000636	-0.000013

CC	Change from survey ΔCC (mm) x	y	z
1	0.275262	-0.046137	-0.125329
2	-0.251751	-0.282098	-0.221106
3	0.884681	-0.475751	0.241571
4	-0.333483	0.764368	0.289743
5	0.096004	-0.388666	0.009030
6	0.012366	-0.402536	-0.119713

Table 3: Results of program trying to minimize the slope between TH6 and TH8.